Available online at www.sciencedirect.com

ScienceDirect

journal homepage: www.elsevier.com/locate/he

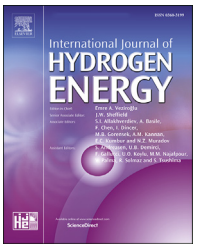

Use of reduced-voltage EIS to establish a relation between oxygen concentration and EIS responses of large commercial PEM fuel cell modules

Babak Ghorbani [a,*], *Jake DeVaal* [b], *Greg Afonso* [b], *Krishna Vijayaraghavan* [a]

[a] *Mechatronic Systems Engineering, Simon Fraser University, Surrey, BC, Canada V3T 0A3*

[b] *Ballard Power Systems, 9000 Glenlyon Parkway, Burnaby, BC, Canada V5J 5J9*

HIGHLIGHTS

- Real and Imaginary parts of EIS scan of different cells add to reconstruct stack EIS signature.
- One can decompose EIS scan of the stack into cell level scans if EIS signature of one cell is known.
- Decreasing oxygen concentration uniquely changes the shape of the LF arc in EIS scan.
- One can use EIS scan of the stack to identify and quantify the hydrogen leak at cell level.

ARTICLE INFO

Article history:
Received 15 March 2023
Received in revised form
24 April 2023
Accepted 27 April 2023
Available online xxx

Keywords:
EIS
Crossover
Injection
Warburg
Oxygen starvation

ABSTRACT

This paper employs equivalent circuit analysis of electrochemical impedance spectra (EIS) signatures of commercial proton exchange membrane fuel cell stacks (PEMFC) to establish a relation between oxygen concentration and EIS response within individual cells of the stack. This paper is part of an ongoing effort to use EIS for detecting and quantifying hydrogen crossover to understand and reduce hydrogen cathode exhaust emissions. Selected results from different sets of experiments performed on Ballard water-cooled and air-cooled PEMFC stacks are presented. A novel reduced-voltage EIS system with the ability to perform impedance measurements over different cell counts is employed to record EIS scans of these stacks. In the first set of experiments, hydrogen was injected into the cathode side of a 30 kW 150+-cell water-cooled module at various rates to emulate the phenomenon of hydrogen crossover at different levels. In the second set of experiments, nitrogen was injected into a target single-cell in an air-cooled stack with over 50 cells (50+-cell) to dilute the cathode available oxygen, and the impedance was measured over various numbers of cells spanning around this target cell. A novel equivalent circuit model with resistors, constant phase elements (CPEs), and a linear finite Warburg parameter was used to study the EIS data via an optimization-based fitting approach in python. Results of these experiments have shown there is a proportional relationship between the Warburg parameter (in the equivalent circuit model used) and hydrogen crossover (at nominal idle and low-current air flows), and that this Warburg parameter increases significantly with reduced cathode air flows. Also, it is concluded that this relationship can be further used,

* *Corresponding author.*
E-mail addresses: bghorban@sfu.ca, babak_ghorbani@sfu.ca (B. Ghorbani).

https://doi.org/10.1016/j.ijhydene.2023.04.323

Please cite this article as: Ghorbani B et al., Use of reduced-voltage EIS to establish a relation between oxygen concentration and EIS responses of large commercial PEM fuel cell modules, International Journal of Hydrogen Energy, https://doi.org/10.1016/j.ijhydene.2023.04.323

along with decomposition of the EIS scan of a stack into different cell-level scans, to estimate the number of large-leaky cells as well as the total hydrogen crossover rate.

Introduction: use of EIS to detect various PEM fuel cell and system faults

Proton exchange membrane fuel cells (PEMFCs) have been gaining in popularity especially in motive applications. The promise that low temperature PEMFCs have shown in power generation with zero emissions, low-noise operation, and fast start-up makes this technology an ideal candidate for automotive applications. Nonetheless, mechanical degradation of components, catalyst aging, and carbon corrosion can adversely affect the durability and performance of fuel cells [1]. Oxygen or fuel starvation within the cells can accelerate these modes of failure [2]. Therefore, detection of such faults are crucial for PEMFCs to achieve high durability and high electrochemical activity at lower costs in order to reach large-scale commercialization [3–6].

Oxygen starvation denotes the condition where an insufficient amount of oxidant is delivered to the catalyst on the cathode (air/oxygen) side. Within the fuel cell, the proton exchange membrane only permits the flow of H_3O^+ ions. As fuel cells are normally connected electrically in series to form "stacks," H_3O^+ migration is forced to occur even when the fuel cell is oxygen starved. However, when the cell is starved, there is insufficient oxygen for H_3O^+ ions to fully participate in the oxygen reduction reaction (ORR). Consequently, there will be a huge loss in power output caused by the drastic reduction in cell voltage. It was shown by Dou et al. [7] that decreasing the air stoichiometry ratio to 0.9 and 0.2, drops the voltage to as low as −0.08 V and −0.2 V, respectively. Furthermore, the unused hydrogen ions can be electrochemically reduced to hydrogen molecules in the absence of oxygen on the cathode side, resulting in cathodic hydrogen emission; this phenomenon is called hydrogen pumping. It may be noted hydrogen pumping can only begin after all the oxygen is fully consumed. It should further be noted that supervisory controls typically maintain and measure sufficient oxygen supply, and oxygen starvation almost always only occurs when the oxygen supply is reduced due to faults such as flow blockage or hydrogen leak faults. Hydrogen leakage is a fault that can further accelerate oxygen starvation. Thus, oxygen starvation, hydrogen leakage, and hydrogen pumping are related to each other as illustrated in Fig. 1. Narimani et al. [8] performed an experimental study on a Ballard 9-cell Mk1100 stack to correlate the cathodic hydrogen emission with oxygen starvation. In their study, Narimani et al. used Riken Keiki Industries (RKI) and Neodym Panterra hydrogen sensors at the cathode outlet to measure the hydrogen concentration while monitoring the voltage on the cell level [8]. They found a strong nonlinear correlation between oxygen concentration and cathodic hydrogen emission [8].

Electrochemical impedance spectroscopy is a powerful non-destructive experimental technique that can distinguish between different physical phenomena occurring at different time scales within the fuel cells [9]. EIS techniques have been applied to PEMFCs to monitor both internal components and external operating conditions. Specifically, many researchers performed a diagnosis of PEMFC operating parameters such as temperature, gas stoichiometry, and water content. EIS can also be employed for the diagnosis of fuel cell components. Due to the numerous applications of EIS, one can find various review studies on the diagnosis of PEMFCs using this technique. Hunsom et al. [10] reviewed different EIS applications along with their principles for studying the effects of operating conditions on the performance of poisoned cells. Gomadam et al. [11] compared various equivalent circuit models (ECMs) for PEMFCs, while Yuan et al. [12] represented in-situ and ex-situ impedance measurements that addressed fuel contamination effects. More recently, Pivac et al. [13] provided a disquisition on potential reasons behind the inductive behavior of PEMFC at the low-frequency range observed in EIS scans. Furthermore, there is a comprehensive review by Rezaeiniya et al. [14] on existing methods for EIS measurement and hardware. A more recent publication by Tang et al. [9] has reviewed several EIS studies for the diagnosis, optimization, and monitoring of PEMFCs in addition to

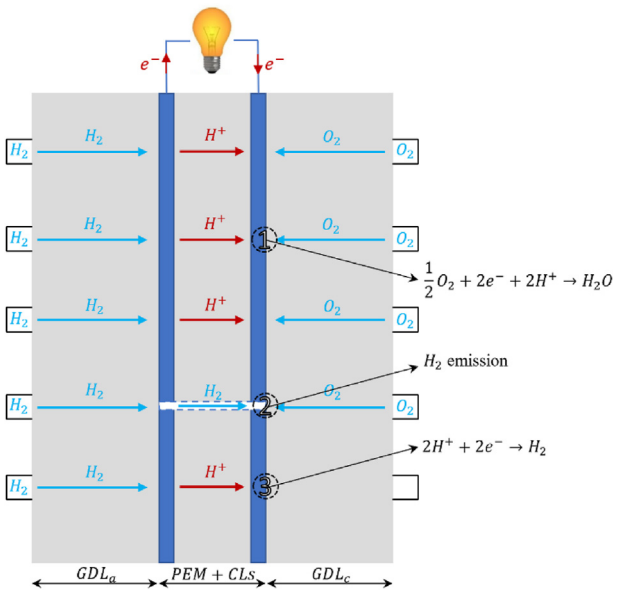

Fig. 1 – Schematic of the proton exchange membrane (PEM), anode/cathode catalyst layers (CLs), and anode/cathode GDL operating with: (1) normal condition, (2) hydrogen cross-over, and (3) oxygen starvation.

Please cite this article as: Ghorbani B et al., Use of reduced-voltage EIS to establish a relation between oxygen concentration and EIS responses of large commercial PEM fuel cell modules, International Journal of Hydrogen Energy, https://doi.org/10.1016/j.ijhydene.2023.04.323

discussing the current challenges in enhancing measurements and diagnosis reliability. More specifically, many researchers performed diagnoses of PEMFC operating parameters such as temperature, gas stoichiometry, and water content. EIS can also be employed for diagnosis of fuel cell components. Table 1 has organized the recent publications on EIS-based analysis of PEMFCs on the basis of their primary diagnosis parameter. This summary and the detailed review below suggest that it would be plausible to find the signatures of oxygen starvation, hydrogen leakage, and more generally mass transfer losses in the EIS plots of fuel cells.

A very common approach to EIS analysis involves finding an equivalent circuit to fit the raw EIS data. In one of the early attempts, EIS scans of a single cell of a PEMFC at different operating conditions were obtained by Aaron et al. [91]. They varied the relative humidity from 0.2 to 0.98, and the temperature from 30 °C to 50 °C while maintaining the air stoichiometry between 1.33 and 2.67 and a constant fuel stoichiometry ratio of 4. The frequency used for obtaining the scans ranged between 0.1 Hz and 100 kHz. They then developed an equivalent circuit consisting of two resistors connected in series with two sets of resistor-capacitor that were connected in parallel [91]. The paper does not provide any details on the effect of the individual elements on the EIS scan. Shan et al. [92] examined the capabilities of microporous layers (MPLs) in removing water from a single cell of a PEMFC. They provide a more detailed and practical equivalent circuit that captured all ohmic losses using a single resistor in series with the rest of the circuit. Three different zones were observed by Shan et al. [92] in their EIS scan of a single cell – a small high frequency (HF) zone due to anode charge transfer loss, a small low frequency (LF) zone which accounts for mass transfer losses, and a relatively large arc in the middle at moderate frequency ranges (MF) representing cathodic charge transfer losses. Another major contribution of this study was the employment of constant phase elements (CPEs) instead of capacitors. The use of CPEs is warranted owing to non-uniform diffusivity in the CL and GDL, and the CPEs achieve a better recreation of EISs arcs that were not fully semi-circular. No information was provided regarding the frequency range of the scans. Shan et al. [92] used EIS as a powerful tool for quantifying different polarization losses within fuel cells and concluded that MPLs can significantly enhance the performance of PEMFCs by facilitating water removal from the cell. In another study, Latorrata et al. [93] successfully evaluated the performance of novel gas diffusion electrodes by employing a Solartron 1260 frequency response analyzer (FRA) for obtaining the EIS scans. An AC signal of 0.2 A was applied along with an RBL488-50-150-800 electric load. The electric circuit had a simple Randles circuit consisting of a resistance in series with a constant phase element–resistor in parallel, and the impedance spectra were fitted using Zview® software. The application of EIS in fuel cells is not limited to performance evaluation at different operating conditions or electrode morphology. Asghari et al. [23] changed the operating temperature as well as the clamping torque of the cell to investigate the effect of non-uniform assembly pressure on EIS scans. Asghari et al. ignored anode activation losses and used a pseudo-inductance in their equivalent circuit model to account for the effects of the current collector plates and metallic components of the cell on EIS at the high-frequency range. One important finding of Asghari et al. [23] is that high-frequency resistance and mass transport resistance also change with changing the clamping torque and assembly pressure due to their effects on interfacial contact resistance.

It is clear from the literature that EIS can play a crucial role in discerning different physical phenomena happening inside a fuel cell stack. This is in part owing to all sources of polarization losses including activation, mass transfer, and ohmic over-potentials revealing their signatures in the impedance

Table 1 – Summary of literature on EIS-based analysis of PEMFCs.

Diagnosis Parameter	Materials Covered	References
Operating Temperature	Effects of operating temperature on: - High-frequency resistance (HFR) - Charge transfer resistance - Gas transport resistance - Water removal	[15–23]
Relative Humidity	Effects of relative humidity on: - Capacitive low-frequency (LF) arcs - Different polarization losses - Water flooding	[24–29]
Gas Stoichiometry and Pressure	Effects of oxygen and hydrogen stoichiometry and operating pressure on: - Different polarization losses - Hydrogen starvation - Oxygen starvation - Water flooding	[30–40]
Water Content	Applications of EIS in the diagnosis of: - Water flooding - Membrane dehydration - Developing water management strategies	[41–49]
Membrane	Using EIS for characterizing optimal membrane materials	[50–52]
Gas Diffusion Layer (GDL)	- EIS sensitivity to membrane materials - Micro porous layer (MPL) effects on EIS - Impacts of carbon loading on EIS	[53–72]
Catalyst Layer (CL)	EIS signatures of ionomer content, loading, and catalyst degradation	[73–90]

Please cite this article as: Ghorbani B et al., Use of reduced-voltage EIS to establish a relation between oxygen concentration and EIS responses of large commercial PEM fuel cell modules, International Journal of Hydrogen Energy, https://doi.org/10.1016/j.ijhydene.2023.04.323

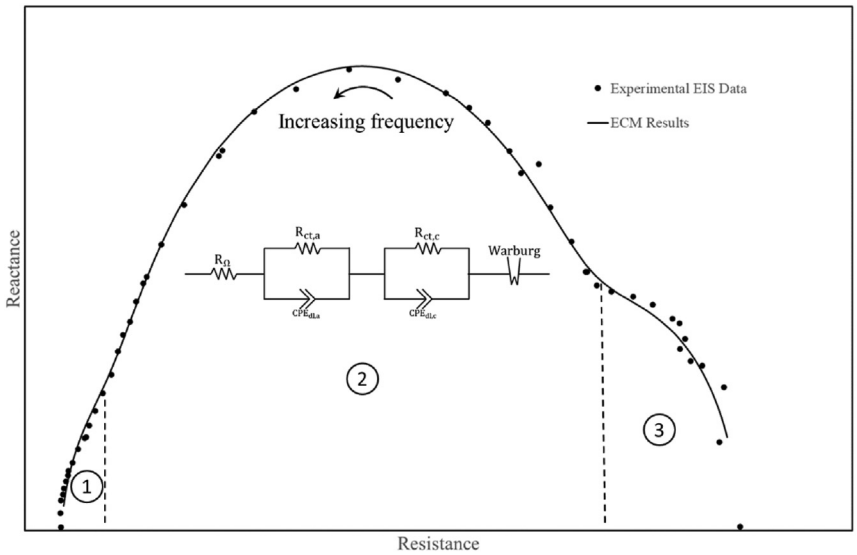

Fig. 2 – A generic experimental EIS scan and the electrical circuit.

spectra. In Fig. 2 a generic EIS scan of a single PEMFC stack operating at a steady state is provided. The valuable information hidden in an EIS plot should be quantified for it to be useful and this has been done by EIS circuit analysis. The ultimate goal in performing EIS circuit analysis is to find an electrical circuit that mimics the behavior of a given EIS curve by producing a similar Nyquist diagram. Rather than examining responses at individual frequencies, changes within the fuel cell (caused by faults) can then be mapped to variations in the EIS parameters. Although each of the circuit elements presents a different source of polarization loss, it should be noted that the fitted circuit should be chosen per electrochemical and physical phenomena taking place inside the fuel cell, because there might be multiple circuit designs with similar responses. The electrical circuit employed by the current study is shown in Fig. 2. More details of the electrical circuit modeling are provided in section Equivalent Circuit Modeling (ECM). As with Shan et al. [92], the EIS scan of a generic fuel cell, or over a series collection of cells in a stack, as shown in Fig. 2, is composed of three characteristic zones that are labeled HF (zone 1), MF (zone 2), and LF (zone 3) generating arcs in the scans. The first two zones represent anodic and cathodic charge transfer losses contributing to the main source of activation overpotential, and quantified by two resistors $R_{ct,a}$ and $R_{ct,c}$ in parallel with constant phase elements. The third arc, which is mathematically modeled by a Warburg element (W), will be the focus of the current study. This arc, which is also called the LF arc of the scan, corresponds to mass transfer losses and is mainly affected by the oxidant (in our case oxygen) concentration distribution along the cathode active area. It is also worth mentioning that the point where the HF crosses the real (horizontal) axis is a measure of fuel cell ohmic overpotential. The (real) value of this intersection point is called the minimum high-frequency resistance (HFR) and is impacted by cell/stack total ohmic losses as well as the membrane water content.

As discussed earlier, there is no literature that cumulatively addresses oxygen starvation, hydrogen emission, and hydrogen pumping in a large stack using EIS. Furthermore, large stacks produce a large output voltage that is too large for traditional EIS measurement instrument. Our current and previous works have obtained the EIS spectra of large stacks using a novel reduced-voltage EIS system [94]. In the current work, the EIS signatures were obtained from two sets of experiments on different cell architectures, studying first the impact of hydrogen crossover on stack-level EIS scans (section Reducing oxygen through hydrogen injection in the 30kW liquid-cooled PEM stack); and secondly, the impact of reduced-oxygen concentration by nitrogen dilution in a single-cell of an air-cooled stack (section Reducing oxygen through nitrogen injection in a single cell of 2 kW air-cooled stack). In the first tests, hydrogen was injected into the cathode inlet flow at different flow rates to study the effects of "reducing the oxygen concentration in all 150+ cells equally" on the EIS response of the stack, and also on the oxygen concentration at the cathode outlet. These experiments were conducted at idle (i.e., 20 A current) and on a Ballard water-cooled 150+ cell stack. Secondly, the oxygen concentration in one air-cooled cell was reduced by injecting nitrogen into the cathode air stream of a single target cell in an air-cooled stack, and EIS scans were obtained over different cell counts up to 50+ cells to understand effects of oxygen starvation at both the cell and stack levels, and to examine how one can connect scans of leaky cells with those of healthy ones in a stack composed of a mixture of healthy and leaky cells. More discussions regarding the ECM are mentioned in section Equivalent Circuit Modeling (ECM) while details of the experiments are presented in section Reducing oxygen through hydrogen injection in the 30kW liquid-cooled PEM stack.

Equivalent circuit modeling (ECM)

Analyzing the Nyquist/EIS plot is one of the most powerful techniques for interpreting impedance data. The PEMFC EIS plot typically consists of one, two, or three arcs depending on

Please cite this article as: Ghorbani B et al., Use of reduced-voltage EIS to establish a relation between oxygen concentration and EIS responses of large commercial PEM fuel cell modules, International Journal of Hydrogen Energy, https://doi.org/10.1016/j.ijhydene.2023.04.323

operating conditions and the microstructure of electrodes. The EIS plot of a generic PEMFC or stack is shown in Fig. 2. According to Fig. 2, there are three loops in the EIS scan of a PEMFC. Note that the points on the very left end of the plot correspond to high frequency, while the frequency decreases as one moves to the right side of the plot (i.e., to the bigger values on the real axis). The first arc on the left end of the EIS plot is called the high frequency (HF) arc, while the ones in the middle and right end are regarded as the medium frequency (MF) and low frequency (LF) arcs, respectively. Each of these arcs/loops represents a physical phenomenon in the fuel cell. All sources of potential loss in the fuel cell, i.e., the charge transfer resistance, mass transport resistance, double layer capacitance in the catalyst layer, and ohmic resistance can be interpreted by the EIS scan. Therefore, quantifying different sources of loss in the fuel cell can be a useful tool for understanding and quantifying the existing faults. This quantification can be done using equivalent circuit modeling (ECM). Different equivalent circuits have been used in the literature to post-process the experimentally obtained EIS scans. The main objective of ECM is to find numerical values of the circuit elements such that the equivalent circuit yields the closest EIS plot to the EIS scan. Hence, ECM is regarded as an optimization problem once the circuit elements are determined. However, one may find many different circuit configurations that provide us with nearly the same EIS plot [95]. For the changes in ECM to be correlated to changes in oxygen concentration (or any other physical phenomenon for that matter), the circuit elements must be based on underlying physical phenomena occurring in the fuel cell [95].

The electrical circuit configuration used for EIS analysis of PEMFCs has changed significantly over time. The first circuit in Fig. 3(a) which was employed by Yan et al. [20] includes three resistors for ohmic resistance, cathodic charge transfer resistance, and mass transfer resistance named R_{Ω}, R_{ct}, and R_{mt}, respectively. In order to take into account the double layer capacitance in the catalyst layer which results in activation losses, constant phase elements were used by Yan et al. [20], The model shown in Fig. 3(a) ignores the anodic charge transfer resistance which is not an inaccurate assumption since cathodic charge transfer loss is more dominant. Intending to quantify the mass transfer losses more accurately, Zhai et al. [96] employed a finite-length Warburg diffusion element shown in Fig. 3(b). A Warburg element is a variation of a constant phase element with a phase of 45° and magnitude proportional to the inverse of the square root of the frequency, while a finite length Warburg is a further variation of the Warburg element to account for finite diffusion length [97]. Since a part of the HF arc lies below the real axis, an inductor was employed by Zhai et al. [96] to account for the inductive behavior of the metallic parts in the fuel cell setup. A nearly similar circuit shown in Fig. 3(c) was used by Wagner et al. [98] in a study in which the Bode diagram was used instead of the EIS plot. Furthermore, Ren et al. [99] studied the inductive behavior of the cell in more detail by using low-frequency and high-frequency inductors. In the current study, a novel circuit shown in Fig. 4 is introduced which takes advantage of all previous models while focusing on mass transfer losses to detect and quantify hydrogen leakage within a PEMFC stack. The resistors represent ohmic resistance R_{Ω}, anodic charge transfer resistance $R_{ct,a}$, and cathodic charge transfer resistance $R_{ct,c}$, respectively. In order to properly fit the circuit to the HF and MF arcs, on the other hand, constant phase elements $CPE_{dl,a}$ and $CPE_{dl,c}$ were used instead of capacitors, on both anode and cathode sides. It should be noted that utilization of Warburg element for quantifying the mass transfer losses is crucial since changing the oxygen concentration on the cathode side, which is the main element of the current study, significantly controls the size of the third LF arc which corresponds to mass transfer losses. The reduction in oxygen concentration, which happens when there is hydrogen leakage, was done through different approaches in this work including injecting hydrogen into the cathode flow (in the liquid-cooled stack testing) and diluting the air flow to the cathode of a single-cell

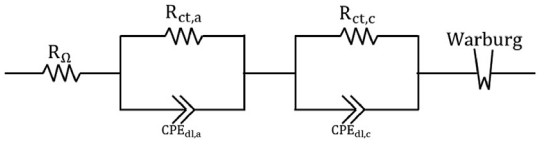

Fig. 4 – Electric circuit used in current work for post-processing of EIS scans.

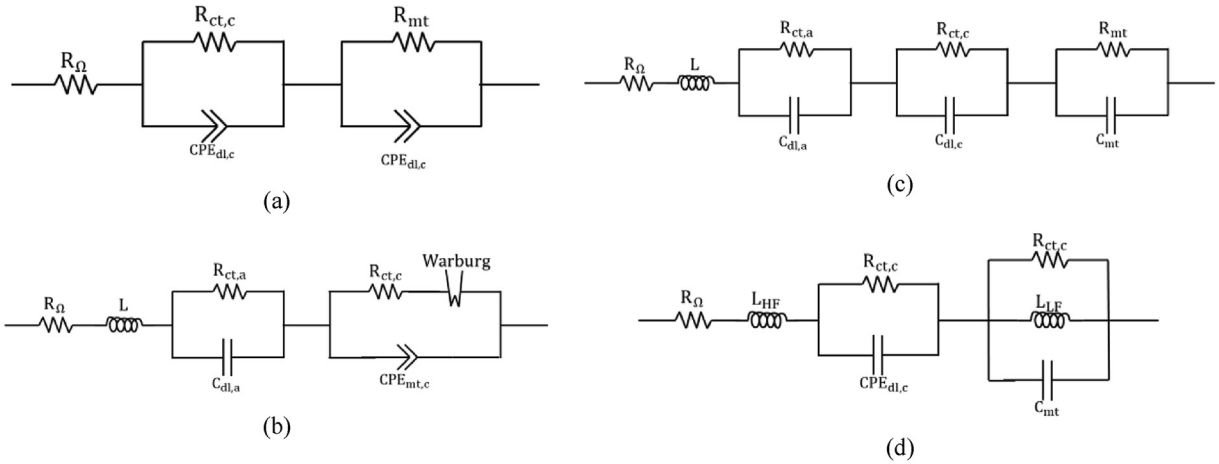

Fig. 3 – The equivalent circuit models employed by (a) Yan et al. [20], (b) Zhai et al. [96], (c) Wagner et al. [98], and (d) Ren et al. [99].

Please cite this article as: Ghorbani B et al., Use of reduced-voltage EIS to establish a relation between oxygen concentration and EIS responses of large commercial PEM fuel cell modules, International Journal of Hydrogen Energy, https://doi.org/10.1016/j.ijhydene.2023.04.323

using nitrogen (in the air-cooled stack testing), where both of these approaches enlarged the third arc of the scan. Since optimization is used for finding the circuit that yields the best fit to the EIS scan, the Warburg element was chosen to be in series with the entire circuit in order to obtain a unique set of solutions. It was observed that non-repetitive and interchangeable results would be found for W and $R_{ct,c}$ while connecting the Warburg element in series to the cathodic charge transfer resistance. No inductors were used since all points below the real axis were ignored when conducting the EIS analysis, and the inductive behavior of the cells/stack was not a concern of this study. The impedance. py library of Python (version 1.5.0) was used along with the Genetic Algorithm (GA) to find the optimal fit to the experimental data.

Reducing oxygen through hydrogen injection in the 30 kW liquid-cooled PEM stack

In this section, a 150+-cell 30 kW liquid-cooled stack was studied as the module was operating at idle (corresponding to 20 A current). Hydrogen was injected downstream of the module air compressor directly into the cathode inlet airflow of the entire stack to emulate the hydrogen crossover phenomenon in every cell in the stack. This injected hydrogen mixes uniformly with the inlet airflow and reduces the available oxygen in all of the cells at the same time. The rate of hydrogen injection was changed from 2 slpm to 48 slpm and EIS plots were generated in a series of tests. Kramers-Kronig (K–K) relations [100] were used to evaluate linearity, causality, and stability of EIS scans and all scans passed the test. The hydrogen injection was periodically turned off, and it was ensured that the new EIS baseline plots of the restabilized fuel cell were identical to the initial baseline. This was done to ensure consistency between experiments as well as to make sure experiments do not cause any permanent damage to the stack or negatively affect the results. EIS scans of the stack at different injection rates are depicted in Figs. 5–7. It should be noted owing to the architecture of the water-cooled stack, it was neither possible to vary the inlet flow of individual cells nor to inject hydrogen into individual cells. It was also infeasible to instrument individual cells. Subsequently, only stack-level EIS was collected here, and cell-level scans were obtained through the second set of experiments performed using the 2 kW air-cooled stack in section Reducing oxygen through nitrogen injection in a single cell of 2 kW air-cooled stack. Fig. 5 shows EIS scans of the liquid-cooled stack for the baseline as well as for cases with 2 slpm to 10 slpm hydrogen injection rates, where the LF arc starts to develop more significantly at 10 slpm hydrogen and higher injection rates. A very interesting phenomenon here is that the mass transfer resistance of the stack with no injection is slightly larger than the mass transfer for cases with 2 slpm and 4 slpm injection rates. The reason for this is believed to be that, at very small hydrogen injection rates, the tiny holes already existing in the membrane are sealed by the water produced due to hydrogen and oxygen recombination. Fig. 6, on the other hand, shows EIS scans at middle-range injection rates from 10 slpm to 25 slpm. Here, the mass transfer arc is still increasing by increasing the injection rate from 10 slpm to 25 slpm hydrogen. Finally, the scans corresponding to high injection rates of up to 45 slpm hydrogen are represented in Fig. 7. Beyond the 48 slpm injection rate, it was impossible to record a scan as the module stopped working due to severe voltage and power loss.

Since there was no change in the LF arc appearing in the stack EIS signature for baseline cases, (with no hydrogen injection) before and after testing, there is believed to be no permanent leak through the membrane introduced due to experimentation. There is also a small third arc in the baseline cases that did not grow, which likely corresponds to the small

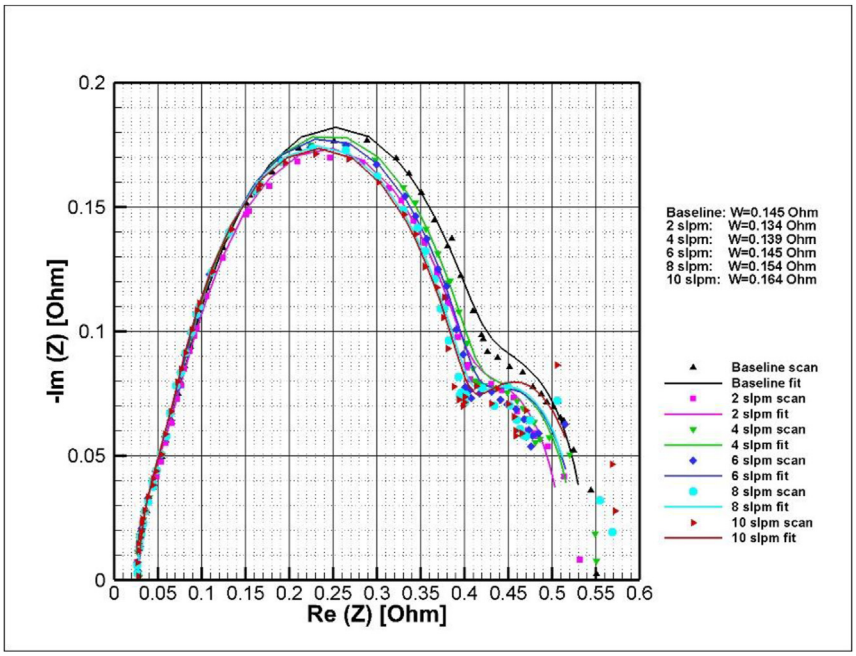

Fig. 5 – EIS signature and the fit to EIS scans for low hydrogen injection rates.

Please cite this article as: Ghorbani B et al., Use of reduced-voltage EIS to establish a relation between oxygen concentration and EIS responses of large commercial PEM fuel cell modules, International Journal of Hydrogen Energy, https://doi.org/10.1016/j.ijhydene.2023.04.323

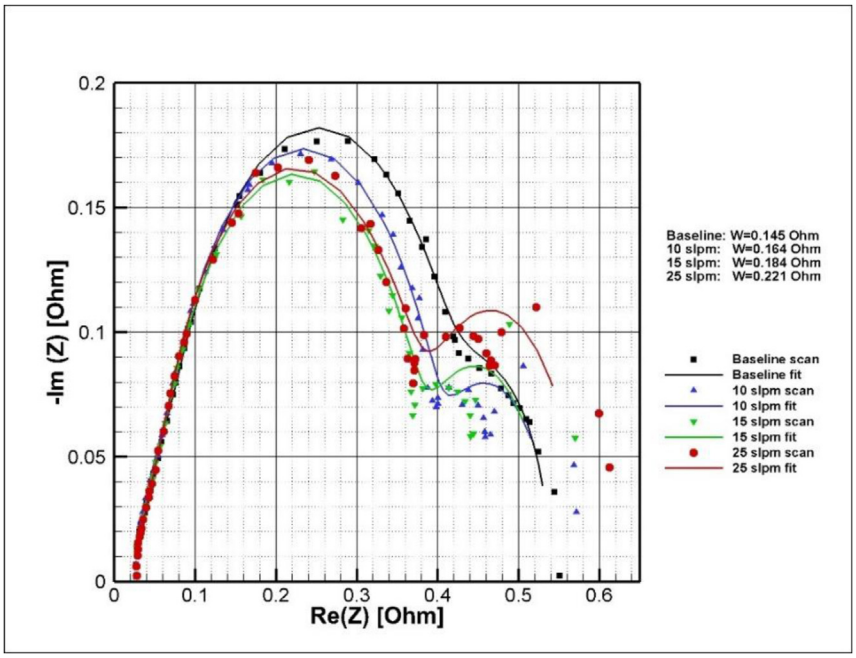

Fig. 6 – EIS signature and the fit to EIS scans for medium hydrogen injection rates.

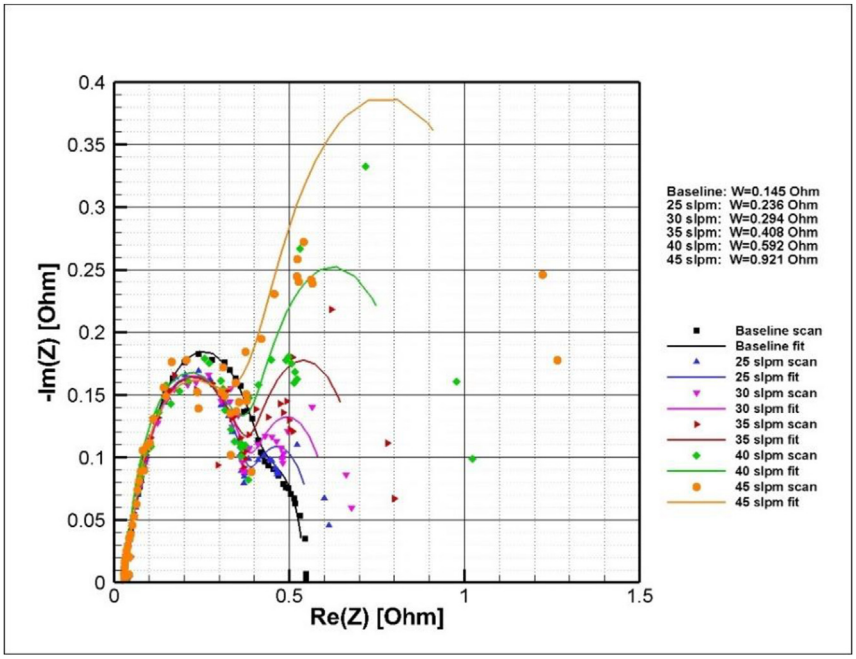

Fig. 7 – EIS signature and the fit to EIS scans for high hydrogen injection rates.

transfer leaks existing in the system before initiating the experiments (again, believed to be below ~2 slpm, because the smallest injection likely seals these leaks via recombination). As hydrogen is injected into the stack cathode under the conditions of a fixed idle airflow, a third arc appears which grows by increasing the injection rate. In tests not reported here, compressor airflow reduction is also seen to result in decreasing stack oxygen stoichiometry. By assuming that all the hydrogen injected and/or transfer-leaked is fully recombined to water in passing through the cells (consuming half of the supplied H_2 flow of oxygen), the effective stoichiometry can be estimated as:

$$\lambda_{O2} = \frac{O_2\ provided}{O_2 consumed} = \frac{\dot{Q}_{O_2.in} - 1/2\left(\dot{Q}_{H_2.inj} + \dot{Q}_{leak}\right)}{1/2 n_{cell} \alpha I} \quad \text{Eq. 1}$$

where:

λ_{O2} is the oxygen stoichiometry (ratio of net O_2 provided to O_2 consumed in sustaining current).

$\dot{Q}_{O_2.in}$ is the compressor dry-input oxygen flow rate (in slpm oxygen).

Please cite this article as: Ghorbani B et al., Use of reduced-voltage EIS to establish a relation between oxygen concentration and EIS responses of large commercial PEM fuel cell modules, International Journal of Hydrogen Energy, https://doi.org/10.1016/j.ijhydene.2023.04.323

$\dot{Q}_{H_2,inj}$ is the stack-level cathode hydrogen injection flow rate (in slpm hydrogen).

$\dot{Q}_{leak}$ is any pre-existing stack-level hydrogen transfer leak rate (in slpm hydrogen).

I is the stack current (in amps),

α is the slpm of hydrogen by the whole stack corresponding to 1 amp of current = 1/2F,

n_{cell} is the number of cells in the stack, and

F is Faraday's constant (in C/slpm).

A quick review and rearrangement of Eq. (1) will show that, if the injected hydrogen flow, Q^i_{H2}, splits up equally amongst the cells, (as should the stack-level oxygen flow, Q^i_{O2}) and any small pre-existing transfer leaks are sealed via recombination of the injected hydrogen to water (i.e., Q^{leak}_{H2} ~ 0), then Eq. (1) can be recast in terms of cell-level oxygen flows and cell-level hydrogen injection/transfer flows. In this state, every cell in the stack would theoretically share the same conditions. Subsequently the real and imaginary parts of stack impedance, Z_{stack}, would be n_{cell} times the real and imaginary parts of a single cell impedance, Z_{cell}.

$$Re(Z_{stack}) = n_{cell} Re(Z_{cell}), Im(Z_{stack}) = n_{cell} Im(Z_{cell}), \quad \text{Eq. 2}$$

As Q^i_{H2}, the hydrogen injection (or simulated leak flow), increases, λ_{O2}, the oxygen stoichiometry will decrease. A stoichiometry below 1, corresponds to more oxygen being consumed in sustaining current than what is available — which is physically impossible. Consequently, in cells with $\lambda_{O2} < 1$, each mole of excess oxygen consumption corresponds to 2 mol of hydrogen emissions, and the total hydrogen emission is given by $\dot{Q}_{H_2,inj} + \dot{Q}_{leak} + n_{cell}\alpha I - 2\dot{Q}_{O_2,in}$. When $\lambda_{O2} > 1$, an alternate form of the calculation for the oxygen concentration at the cathode outlet can be calculated by conducting a mass balance over the entire cathode side from Eq. (1). The flow diagram of the cathode side with hydrogen injected into the inlet is depicted in Fig. 8. According to Fig. 8, the oxygen concentration at the outlet can be calculated as a function of the stack current, the cathode air flow rate, the hydrogen injection rate, and any permanent leak rate by the following expression:

$$X_{O_2,out} = \frac{X_{O_2,in}\,\dot{Q}_a - \frac{1}{2}\left(\dot{Q}_{H_2,inj} + \dot{Q}_{leak}\right) - \frac{\alpha I n_{cell}}{2}}{\dot{Q}_a + \frac{1}{2}\left(\dot{Q}_{H_2,inj} + \dot{Q}_{leak}\right) + \frac{\alpha I n_{cell}}{2}} \quad \text{Eq. 3}$$

One should note that not all water at the cathode outlet is in the gaseous phase and the above formula requires some correction. The maximum amount of water vapor allowed to exist at the cathode outlet flow is determined at the fully humidified condition:

$$RH = \frac{X_{H_2O(v)} P_c}{P_{sat}(T_{cell})} = 1 \quad \text{Eq. 4}$$

Where RH represents relative humidity and $P_{sat}(T_{cell})$ is the saturation pressure of water at cell temperature. The maximum allowed concentration of water vapor is then found by the following expression:

$$X_{H_2O(v)} = \frac{P_{sat}(T_{cell})}{P_c} \quad \text{Eq. 5}$$

Therefore, the amount of water vapor present at the cathode outlet is:

$$\dot{Q}_{H_2O(v)} = \frac{X_{H_2O(v)}}{1 - X_{H_2O(v)}} \dot{Q}_{others} \quad \text{Eq. 6}$$

Where $\dot{Q}_{others}$ represents the flow rate of oxygen and nitrogen at the outlet. Finally, after some simplifications, the oxygen concentration at the cathode outlet is given as follows:

$$X_{O_2,out} = \frac{2X_{O_2,in}\,\dot{Q}_a - \left(\dot{Q}_{H_2,inj} + \dot{Q}_{leak} + \alpha I n_{cell}\right)}{2\dot{Q}_a - \left(\dot{Q}_{H_2,inj} + \dot{Q}_{leak} + \alpha I n_{cell}\right)} \left(1 - \frac{P_{sat}(T_{cell})}{P_c}\right) \quad \text{Eq. 7}$$

Note that P_{sat} is calculated using the following formula [101]:

$$\ln P_{sat}(T_{cell}) = -34.625 + 0.258\,T_{cell} - 4.8419 \times 10^{-4}\,T^2_{cell} + 3.3282 \times 10^{-7}\,T^3_{cell} \quad \text{Eq. 8}$$

The oxygen concentration at the cathode outlet was measured experimentally in the injection tests using a NOVA oxygen sensor. The relationship between the Warburg parameter and measured oxygen concentration at the cathode outlet for our set of hydrogen injection tests is presented in Fig. 9. Here, one can see that reducing the oxygen concentration affects the LF arc of the stack scan. As seen in Fig. 9, a second-degree polynomial fits the data very well. As, a result, one can potentially quantify the cell-level hydrogen leak if the Warburg value is found using EIS. Such an approach, however,

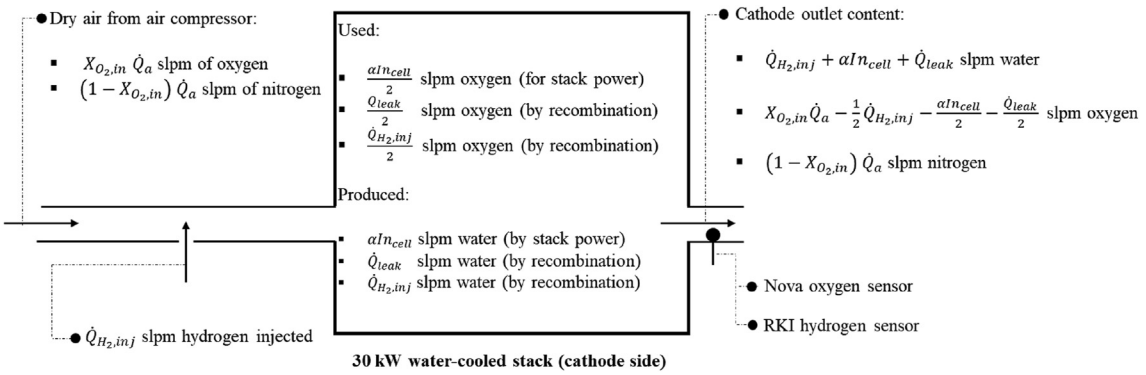

Fig. 8 – Mass balance over the entire stack (cathode side).

Please cite this article as: Ghorbani B et al., Use of reduced-voltage EIS to establish a relation between oxygen concentration and EIS responses of large commercial PEM fuel cell modules, International Journal of Hydrogen Energy, https://doi.org/10.1016/j.ijhydene.2023.04.323

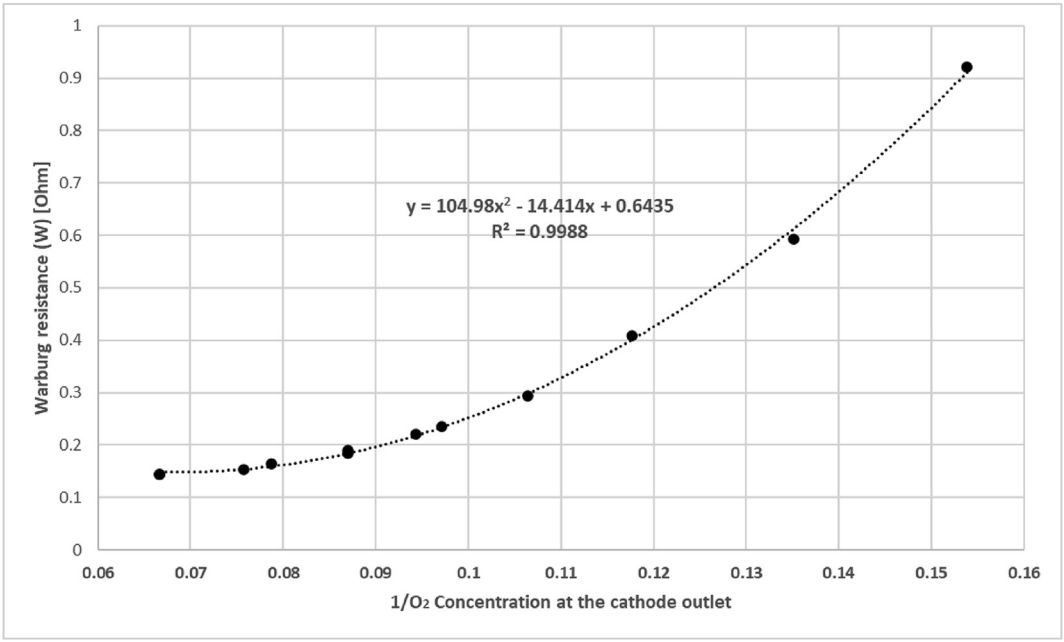

Fig. 9 – Relationship between the Warburg resistance and measured oxygen concentration at the cathode outlet (for EIS scans performed on a water-cooled 150+-cell stack at idle-level air flows (4.5–4.7 g/s) and currents (20.0–20.8 A).

Table 2 – Experimental values for oxygen concentrations at the cathode outlet for a set of experiments performed on the water-cooled stack.

Test name	Air flow rate (gr/s)	Minimum O_2 concentration (%)	Measured O_2 concentration (%)	Maximum O_2 concentration (%)	Stack current (A)
Baseline 1	4.69	14.6	14.9	15.7	20.8
Baseline 2	4.72	14.6	15.0	15.7	20.8
Baseline 3	4.74	14.6	14.9	15.7	20.9
Baseline 4	4.54	14.6	15.0	15.7	20.0
2 slpm H_2	4.55	14.2	14.5	15.3	20.0
4 slpm H_2	4.54	13.8	14.0	14.8	20.0
6 slpm H_2	4.55	13.4	13.6	14.4	20.0
8 slpm H_2	4.54	13.0	13.2	13.9	20.0
10 slpm H_2	4.55	12.6	12.7	13.5	20.0
10 slpm H_2	4.70	12.6	12.7	13.6	20.8
15 slpm H_2	4.67	11.5	11.5	12.4	20.8
20 slpm H_2	4.71	10.6	11.3	11.4	20.8
5.0% ACS	3.19	12.2	12.7	13.1	20.3
4.5% ACS	2.47	10.0	10.2	10.7	20.0
4.0% ACS	1.85	6.6	6.9	7.1	19.6

requires knowledge about how cell-level EIS scans of leaky and normal cells combine with stack-level EIS scans; where this would require information on the distribution of cell-level transfer leaks in a stack [102], or at a minimum, the presence of a single leaky-cell whose size can be adjusted. To further develop this idea, another set of experiments was performed on an air-cooled stack by injecting nitrogen in a single cell to reduce the oxygen concentration and obtaining EIS scans at both a cell level and over larger cell-counts spanning the starved cell.

As mentioned previously, not all water leaving the stack would be in the vapor phase, while the amount of vapor water is limited to the case of a hundred percent relative humidity, depending on the operating temperature. Therefore, the most accurate practice to take is to provide a possible range for oxygen concentration corresponding to values of relative humidity changing between 0 and 100%, with the goal for the oxygen sensor readings to then fall within the range given by the mass balance. The last set of rows in Table 2 corresponds to three separate experiments performed while lowering the air compressor speed (ACS) from 5.0%, 4.5%, and 4% of full compressor speed respectively. Minimum oxygen concentration refers to the case where air is at 100% relative humidity while the maximum corresponds to dry cathode flow if all water stays in liquid form. Based on the results, showing that the measured oxygen sensor readings fall well within the calculated range, the modeling captures the impact of stack current and injection recombination well, and the measured

Please cite this article as: Ghorbani B et al., Use of reduced-voltage EIS to establish a relation between oxygen concentration and EIS responses of large commercial PEM fuel cell modules, International Journal of Hydrogen Energy, https://doi.org/10.1016/j.ijhydene.2023.04.323

data also show that the oxygen sensor readings were fairly accurate.

It should be noted that two hydrogen sensors were placed at the cathode outlet to capture hydrogen emissions from the cathode. Although the hydrogen injection tests resulted in significantly increasing mass transfer losses, significant hydrogen emission (>~0.5% H2) was not observed. This can be attributed to the absence of a large (permanent) leak in the stack, wherein reducing the oxygen concentration had imposed an equal starvation risk to all cells. Specifically, the inlet flows were identical in the cells. Had oxygen concentration been reduced to the level where emission may have occurred, all cells would have simultaneously air-starved, and the entire stack voltage would have become zero or slightly negative. This would have resulted in the stack shutting down due to low voltage. Thus, while injecting hydrogen into the entire stack makes it easier to observe changes in the EIS signature, one of the limitations of this approach is our inability to simulate hydrogen emissions directly. Another limitation of these tests is their inability to simulate leaks in a subset of the cells. As such, these tests alone do not help us understand the effect of leak count or unequal leak rates on the EIS signature and vice versa. To complete the study, the next section provides another set of experiments that were performed on an air-cooled stack with the capability of capturing EIS scans at different cell counts.

Reducing oxygen through nitrogen injection in a single cell of 2 kW air-cooled stack

In this second set of experiments, as shown in the photograph and schematic in Figs. 10 and 11 respectively, nitrogen was injected into the cathode airflow of a specific target cell in the middle of a 50+-cell 2 kW air-cooled PEM stack (to reduce its oxygen concentration by dilution). This dilution-based concentration reduction was necessary because injection of hydrogen into the larger cathode flow channels of air-cooled stacks would give poor recombination, and the potential for autoignition (where the thinner cells used in liquid-cooled

Fig. 10 – Photograph showing polyurethane hose-manifold used to deliver nitrogen through 0.050″ stainless tubing to individual cathode flow grooves in target air-cooled cell.

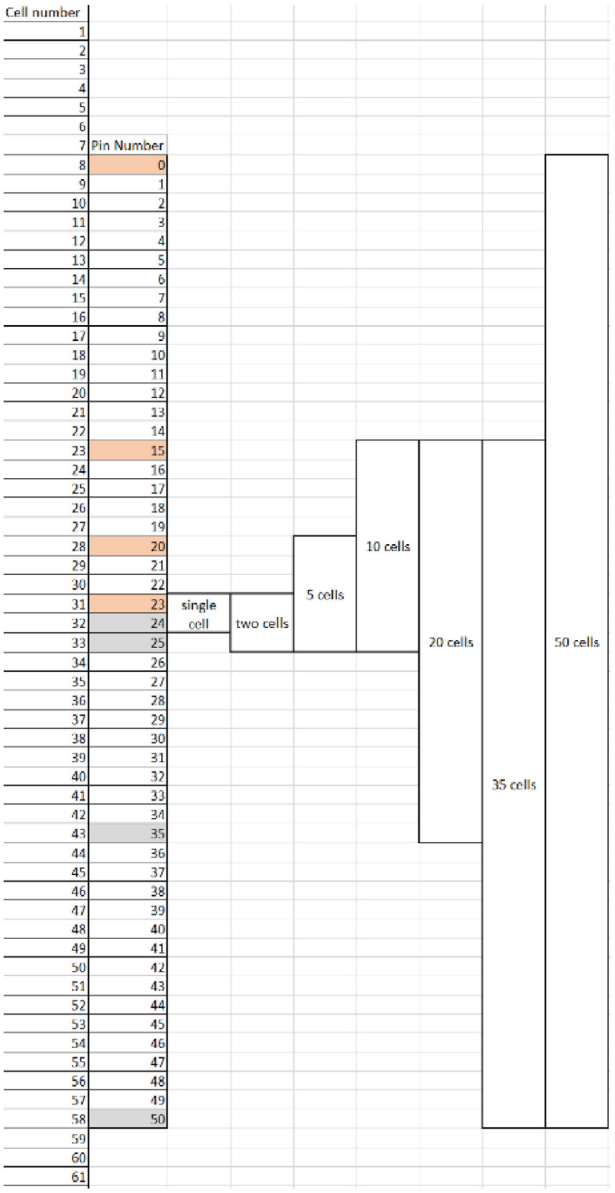

Fig. 11 – Multiplexer configuration.

stacks in section Reducing oxygen through hydrogen injection in the 30kW liquid-cooled PEM stack are not prone to flame transmission). A multiplexer was used to route the EIS sense lines from a Kikisui KFM2150 high voltage EIS system to pairs of cells in the stack, where Fig. 11 shows a map of the multiplexer setup. On the left of Fig. 11 is the stack with its individual cells numbered, where nitrogen is injected into the cathode of cell 31. To the right of Fig. 11 are the EIS measurement pin-pairs starting with the nitrogen-infused cell and spanning 2, 5, 10, 20, 35, and 50 cells; where the specific cell pairs measured were: (31,32), (31,33), (28,33), (23, 33), (23, 43), (23,58) and (8,58).

The nitrogen injected was varied from 25 slpm to 85 slpm to simulate different extents of dilution. Since the individual cells in the stack are electrically in series, their impedances would be additive. Hence, it is hypothesized that the EIS response of cells would be additive. To test this hypothesis,

Please cite this article as: Ghorbani B et al., Use of reduced-voltage EIS to establish a relation between oxygen concentration and EIS responses of large commercial PEM fuel cell modules, International Journal of Hydrogen Energy, https://doi.org/10.1016/j.ijhydene.2023.04.323

EIS scans for multiple cell counts were simulated using the following steps.

a) Baseline EIS data was obtained for the target cell as well as 2/5/10/20/35/50 cells spanning the target cell (for zero injected nitrogen).
b) Experimental EIS data was obtained for the target as well as 2/5/10/20/35/50 cells spanning the target cell for different flow rates of nitrogen (in the range of 25 slpm to 85 slpm).
c) The change (increase) in the impedance of the target cell was calculated for the different flow rates of nitrogen (See Fig. 17 for graph of results.).
d) The EIS responses of 2/5/10/20/35/50 (or 'n') cells with reduced oxygen concentration for different nitrogen injection rates were simulated by adding the impedance change of the target cell corresponding to nitrogen injection (from step c) to '(n-1)' of the baseline cell-impedance(s) for the corresponding cell scan (from step a).

Experimental and simulated EIS signatures of the stack for different numbers of cells at nitrogen injection rates of 25–85 slpm are depicted in Figs. 12–16 respectively. The figures generally indicate good agreement between the experimental and simulated EIS signatures confirming our "addition" hypothesis; with the only exceptions being at cell counts higher than 20 for lower N2 dilution flows (e.g., 25 to 40 slpm).

Let us take a closer look at Fig. 12 corresponding to the cases where membrane leak rates are relatively small. In this figure, it was noticed that there are no discernible third arcs for the 20/35/50 cell-count EIS scans. This is because the third arc of the single leaky cell is so small that it nearly vanishes when being added to the scans of many more healthy cells. Progressing from nitrogen injection rates of 25–55 slpm in Figs. 12–16, it is seen that we can begin to discern the third arc at higher cell spans. While this might initially be considered a potential shortcoming of stack-level EIS for capturing a leaky cell (or multiple leaky cells), a quick review of Eq. (1) shows that, intentionally reducing the airflow to the stack (i.e., move to a lower Q^{i}_{O2} for our testing), the size of the third-arc for the leak-affected cells increases, and this improves our ability to 'find' leaky cells in a larger population. This, and/or the actual development of a higher leak rate in a single cell like shown here, or by more than one cell

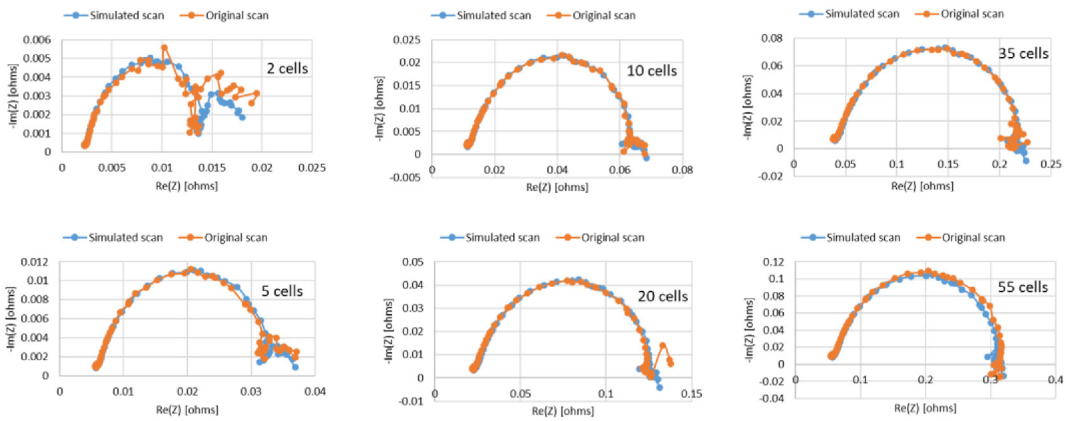

Fig. 12 – Simulated and experimental EIS scans of different cell-counts at 25 slpm nitrogen injection rate.

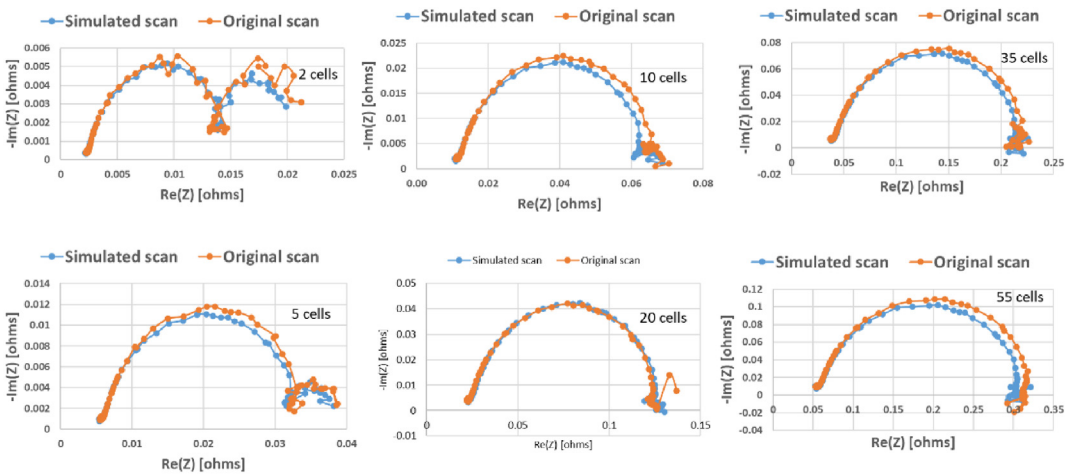

Fig. 13 – Simulated and experimental EIS scans of different cell-counts at 40 slpm nitrogen injection rate.

Please cite this article as: Ghorbani B et al., Use of reduced-voltage EIS to establish a relation between oxygen concentration and EIS responses of large commercial PEM fuel cell modules, International Journal of Hydrogen Energy, https://doi.org/10.1016/j.ijhydene.2023.04.323

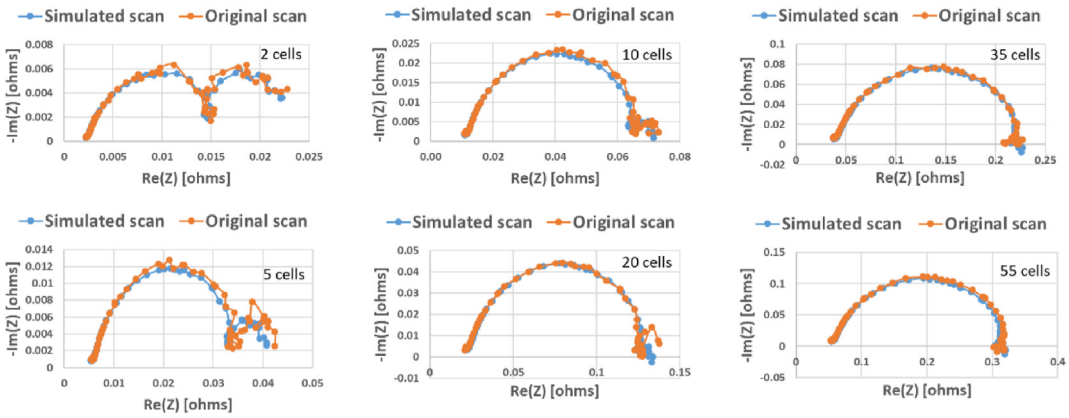

Fig. 14 – Simulated and experimental EIS scans of different cell-counts at 55 slpm nitrogen injection rate.

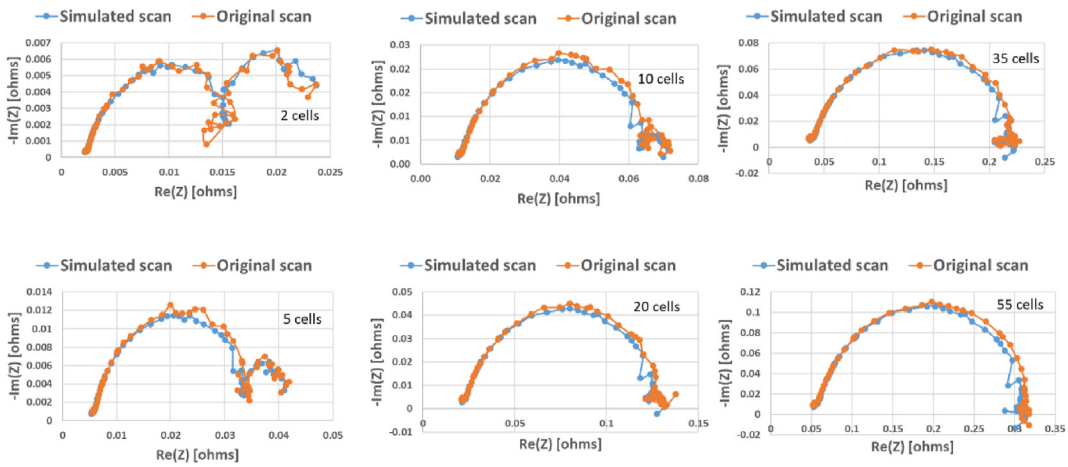

Fig. 15 – Simulated and experimental EIS scans of different cell-counts at 70 slpm nitrogen injection rate.

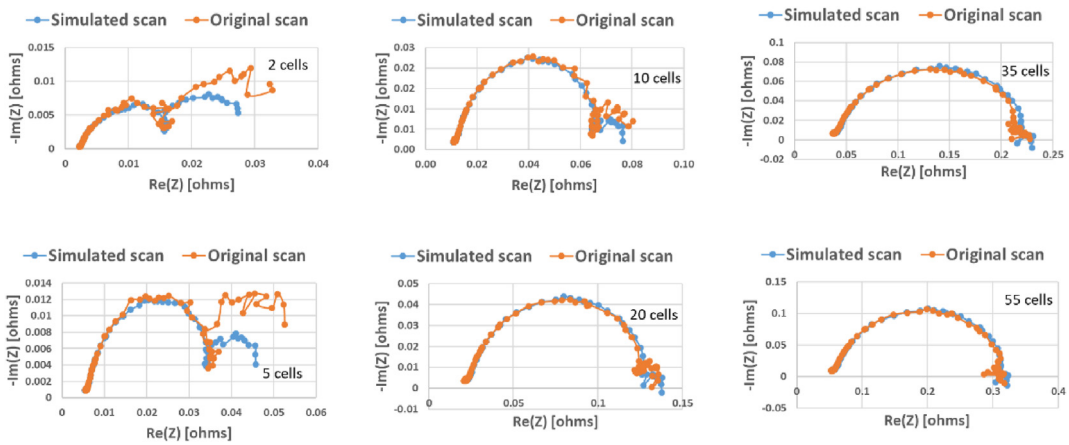

Fig. 16 – Simulated and experimental EIS scans of different cell-counts at 85 slpm nitrogen injection rate.

contributing at lower leak levels (which has not been validated but seems reasonable) is the subject of our future research. To further understand the behavior of EIS scans at the stack level, simulations were performed to see if we can capture the stack-level EIS scan of multiple cells by adding up the EIS signatures of single cells. According to the information provided in Figs. 12–16, this "additivity" feature of EIS scans is validated to a considerable extent. There was only one case corresponding to the 85 slpm nitrogen injection rate shown in Fig. 16, in which the size of the LF arc given by the experiment is larger than what the simulation offers. This can be justified since at this very high injection rate, part

Please cite this article as: Ghorbani B et al., Use of reduced-voltage EIS to establish a relation between oxygen concentration and EIS responses of large commercial PEM fuel cell modules, International Journal of Hydrogen Energy, https://doi.org/10.1016/j.ijhydene.2023.04.323

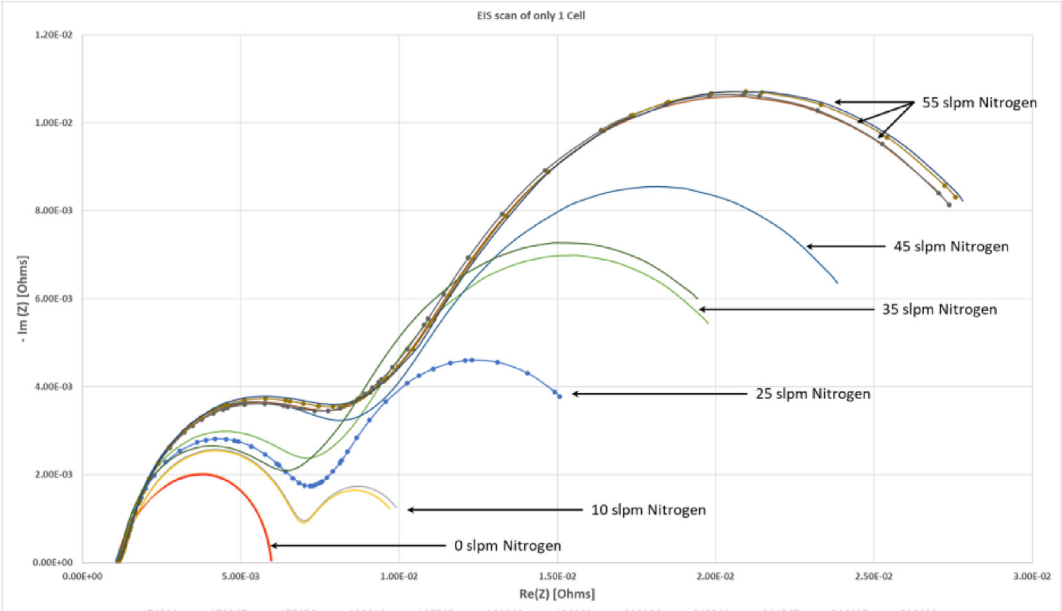

Fig. 17 – Fits to the EIS scans over a single cell at different leak levels (nitrogen injection rate from 0 to 55 slpm).

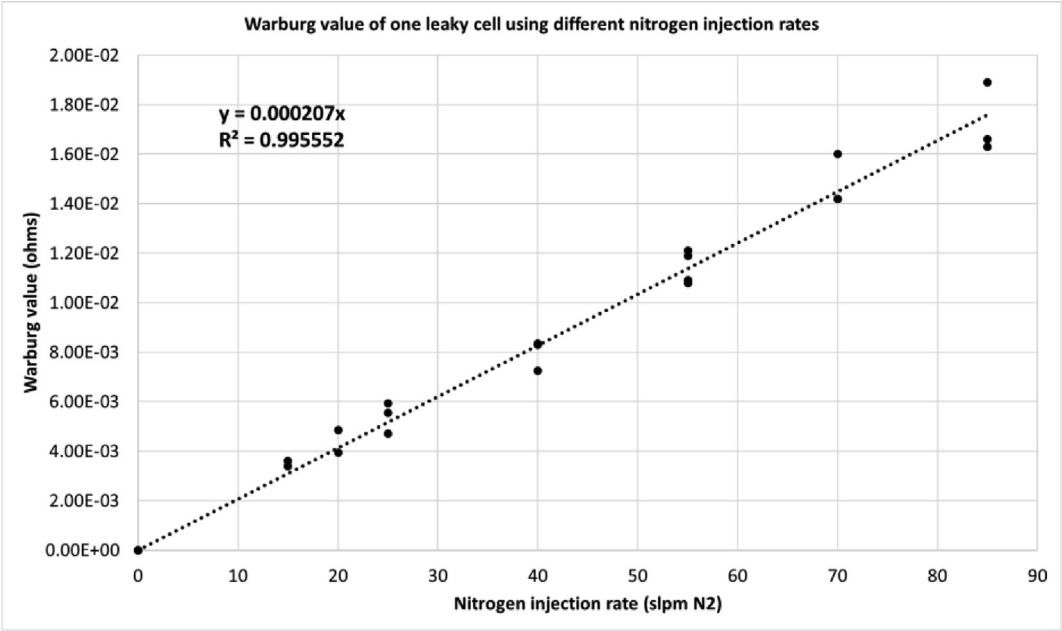

Fig. 18 – Warburg value of one leaky cell at different leak levels representing the size of the low-frequency arc in the EIS scan.

of the nitrogen might have leaked through the neighboring cells causing more dilution.

The gradual appearance of the third arc resulting from the mass transfer losses in only one cell is depicted in Fig. 17. As shown in Fig. 17, the less oxygen available at the cathode catalyst layer caused by injecting nitrogen, the larger the LF arc will be. The size of this LF arc which is quantified by the finite length Warburg element in circuit analysis, therefore, will grow at higher leak rates. To further elaborate on this, the relationship between the nitrogen injection rate (hypothetically the leak rate) and the Warburg resistance is depicted in Fig. 18 which shows a linear connection between the two. Using this relationship in our future studies, the extent of leakage once the cell-level EIS of the leaky cell is found using the decomposition of the stack-level EIS can be quantified.

Results of the electrical circuit analysis performed by fitting the circuit shown in Fig. 4 to the EIS scans of the air-cooled stack are shown in Table 3. Based on the results, there is no significant change in charge transfer resistance and ohmic resistance during experimentation when keeping the number of cells constant. Therefore, reducing the oxygen concentration for emulating the leak phenomenon mostly

Please cite this article as: Ghorbani B et al., Use of reduced-voltage EIS to establish a relation between oxygen concentration and EIS responses of large commercial PEM fuel cell modules, International Journal of Hydrogen Energy, https://doi.org/10.1016/j.ijhydene.2023.04.323

Table 3 – Electrical circuits fitted to the experimental data.

Number of cells	Ohmic resistance (ohms)	Charge transfer resistance (ohms)	Mass transfer resistance (ohms)	Nitrogen injection rate (slpm)	Number of cells	Ohmic resistance (ohms)	Charge transfer resistance (ohms)	Mass transfer resistance (ohms)	Nitrogen injection rate (slpm)
1	1.11E-03	4.89E-03	3.79E-39	0	10	1.09E-02	5.37E-02	8.80E-03	55
1	1.12E-03	5.52E-03	7.55E-03	25	10	1.08E-02	5.44E-02	8.32E-03	70
1	1.11E-03	5.50E-03	8.32E-03	40	10	1.08E-02	5.21E-02	2.00E-02	85
1	1.14E-03	5.47E-03	1.33E-02	55	20	2.19E-02	1.03E-01	1.47E-38	25
1	1.12E-03	6.09E-03	1.18E-02	70	20	2.10E-02	1.07E-01	1.47E-39	55
1	1.13E-03	6.15E-03	1.54E-02	85	20	2.09E-02	1.08E-01	4.55E-56	70
2	2.28E-03	9.85E-03	8.28E-03	25	20	2.08E-02	1.02E-01	1.62E-02	85
2	2.25E-03	1.01E-02	1.05E-02	40	35	3.78E-02	1.78E-01	4.76E-44	25
2	2.25E-03	1.08E-02	1.19E-02	55	35	3.72E-02	1.82E-01	4.37E-53	40
2	2.20E-03	1.07E-02	1.25E-02	70	35	3.70E-02	1.83E-01	1.19E-47	55
2	2.22E-03	1.03E-02	2.49E-02	85	35	3.62E-02	1.83E-01	1.26E-54	70
5	5.58E-03	2.52E-02	6.95E-03	25	35	3.68E-02	1.77E-01	1.25E-02	85
5	5.51E-03	2.60E-02	8.65E-03	40	50	5.43E-02	2.64E-01	1.02E-39	0
5	5.51E-03	2.70E-02	1.21E-02	55	50	5.44E-02	2.59E-01	1.36E-42	25
5	5.43E-03	2.67E-02	1.16E-02	70	50	5.33E-02	2.64E-01	1.05E-42	40
5	5.46E-03	2.58E-02	2.81E-02	85	50	5.27E-02	2.64E-01	1.31E-38	55
10	1.11E-02	5.15E-02	5.08E-03	25	50	5.19E-02	2.63E-01	5.86E-45	70
10	1.10E-02	5.28E-02	5.95E-03	40	50	5.27E-02	2.57E-01	8.75E-50	85

affected the third (LF) arc of multiple-cell scans. There is also changes in the size of the second arc due to changes in charge transfer resistance as a result of water buildup which is in accordance with the very recent findings of other studies [102–107]. Both charge transfer and mass transfer are subject to changes while there are factors other than hydrogen cross-over that would cause the second arc to vary in size [107]. Furthermore, non-zero Warburg parameter values for 20- and 35-cell scans were only obtained at a high nitrogen injection rate of 85 slpm. In conclusion, membrane leakage can be detected in the multiple-cell EIS scan of an air-cooled stack (operating at nominal airflow) only when the leak rate is significantly high if a fair percentage of cells (1/35, or > 3%, in this case) is leaking. No leakage could be detected using an EIS scan over 50 cells when having only one leaky cell, where this is most-likely due to the higher air-stoichiometry (100–200) used in this air-cooled stack versus the lower air stoichs (1.8–4.0) used in the liquid-cooled stack. Here, as mentioned previously however, if the stack airflow is reduced, the size of the third arc for a given leak-size will increase, and improve the sensitivity of the technique.

Conclusion

This paper provides a detailed analysis of the relation between stack oxygen concentration and EIS parameters using two sets of experiments to simulate hydrogen leaks. The first set of experiments was performed on a commercial 30 kW water-cooled PEMFC stack from Ballard. Here, different rates of hydrogen were directly injected into the cathode inlet flow of the whole stack. Increasing the hydrogen injection rate (hypothetically the leak rate) was seen to enlarge the third (LF) arc of the stack EIS signatures and a corresponding increase in the Warburg parameter in the equivalent circuit. The second set of experiments was conducted on a 2 kW air-cooled stack from Ballard. Here different rates of nitrogen were injected into a single cell of the stack, to reduce the oxygen concentration through dilution, and EIS scans were obtained across different cell spans. The results indicated that increasing the nitrogen injection rate also enlarges the third arc of the EIS signatures and a corresponding increase in the Warburg parameter in the equivalent circuit. The results also showed that the EIS scans were generally additive, wherein EIS scans of different cells in a stack can be added to obtain the EIS scan of the stack. This result is significant as it paves the way for our future extension of this work that would aim to decompose the stack-level EIS into cell-level scans, and eventually obtain the number of leaky cells as well as the amount of hydrogen leak rate.

Next steps in this research include performing EIS scans and hydrogen emissions measurements on stacks containing significantly-leaky cells (potentially air-starved) installed in the 30 kW module, and determining the number and size of these leaky-cells by hydrogen/nitrogen characterization [108]. These steps will be used to further investigate the additivity principle demonstrated in the present work, and to develop a methodology for reduced airflow testing that should capture both developing transfer and end-of-life transfer resulting in cathode hydrogen emissions.

Declaration of competing interest

The authors declare that they have no known competing financial interests or personal relationships that could have appeared to influence the work reported in this paper.

Acknowledgments

The authors would like to acknowledge Ballard Power Systems, Burnaby, BC, Canada for facilitating the experimental

Please cite this article as: Ghorbani B et al., Use of reduced-voltage EIS to establish a relation between oxygen concentration and EIS responses of large commercial PEM fuel cell modules, International Journal of Hydrogen Energy, https://doi.org/10.1016/j.ijhydene.2023.04.323

validation. The supervising author would like to acknowledge the funding from Mitacs through Accelerate Grants (IT17289, IT27467) and Discovery Grant (RGPIN/02971-2021) that enabled this research.

REFERENCES

[1] Ghorbani B, Vijayaraghavan K. A review study on software-based modeling of hydrogen-fueled solid oxide fuel cells. Int J Hydrogen Energy 2019;44(26):13700–27.
[2] Ghorbani B, Vijayaraghavan K. Developing a virtual hydrogen sensor for detecting fuel starvation in solid oxide fuel cells using different machine learning algorithms. Int J Hydrogen Energy 2020;45(51):27730–44.
[3] Gatto I, Carbone A, Saccà A, Passalacqua E, Oldani C, Merlo L, Sebastián D, Aricò AS, Baglio V. Increasing the stability of membrane-electrode assemblies based on Aquivion® membranes under automotive fuel cell conditions by using proper catalysts and ionomers. J Electroanal Chem 2019;842:59–65.
[4] Nandjou F, Poirot-Crouvezier JP, Chandesris M, Blachot JF, Bonnaud C, Bultel Y. Impact of heat and water management on proton exchange membrane fuel cells degradation in automotive application. J Power Sources 2016;326:182–92.
[5] St-Pierre J, Myers DJ, Borup RL. Preface—focus issue on proton exchange membrane fuel cell (PEMFC) durability. J Electrochem Soc 2018;165(6). Y7–Y7.
[6] Brunetto C, Moschetto A, Tina G. PEM fuel cell testing by electrochemical impedance spectroscopy. Elec Power Syst Res 2009;79(1):17–26.
[7] Dou M, Hou M, Liang D, Shen Q, Zhang H, Lu W, Shao Z, Yi B. Behaviors of proton exchange membrane fuel cells under oxidant starvation. J Power Sources 2011;196(5):2759–62.
[8] Narimani M, Devaal J, Golnaraghi F. Hydrogen emission characterization for proton exchange membrane fuel cell during oxygen starvation - Part 1: low oxygen concentration. Int J Hydrogen Energy 2016;41(8):4843–53.
[9] Tang Z, Huang QA, Wang YJ, Zhang F, Li W, Li A, Zhang L, Zhang J. Recent progress in the use of electrochemical impedance spectroscopy for the measurement, monitoring, diagnosis and optimization of proton exchange membrane fuel cell performance. J Power Sources 2020;468:228361.
[10] Hunsom M. Electrochemical impedance spectroscopy (EIS) for PEM fuel cells. Spectroscopic properties of inorganic and organometallic compounds. 2011.
[11] Gomadam PM, Weidner JW. Analysis of electrochemical impedance spectroscopy in proton exchange membrane fuel cells. Int J Energy Res 2005;29(12):1133–51.
[12] Yuan X, Wang H, Colin Sun J, Zhang J. AC impedance technique in PEM fuel cell diagnosis-A review. Int J Hydrogen Energy 2007;32(17):4365–80.
[13] Pivac I, Barbir F. Inductive phenomena at low frequencies in impedance spectra of proton exchange membrane fuel cells – a review. J Power Sources 2016;326:112–9.
[14] Rezaei Niya SM, Hoorfar M. Study of proton exchange membrane fuel cells using electrochemical impedance spectroscopy technique - a review. J Power Sources 2013;240:281–93.
[15] Shao H, Qiu D, Peng L, Yi P, Lai X. In-situ measurement of temperature and humidity distribution in gas channels for commercial-size proton exchange membrane fuel cells. J Power Sources 2019;412:717–24.
[16] Roy SK, Orazem ME. Graphical estimation of interfacial capacitance of PEM fuel cells from impedance measurements. J Electrochem Soc 2009;156(2):B203.
[17] Tang Y, Zhang J, Song C, Liu H, Zhang J, Wang H, Mackinnon S, Peckham T, Li J, McDermid S, Kozak P. Temperature dependent performance and in situ AC impedance of high-temperature PEM fuel cells using the nafion-112 membrane. J Electrochem Soc 2006;153(11):A2036.
[18] Asghari S, Ashraf Khorasani MR, Dashti I. Investigation of self-humidified and dead-ended anode proton exchange membrane fuel cell performance using electrochemical impedance spectroscopy. Int J Hydrogen Energy 2016;41(28):12347–57.
[19] Pistono A, Rice-York CA, Boovaragavan V. Electrochemical impedance spectroscopy detection of saturation level in a frozen polymer electrolyte membrane fuel cell. J Electrochem Soc 2011;158(2):B233.
[20] Yan X, Hou M, Sun L, Liang D, Shen Q, Xu H, Ming P, Yi B. AC impedance characteristics of a 2 KW PEM fuel cell stack under different operating conditions and load changes. Int J Hydrogen Energy 2007;32(17):4358–64.
[21] Pivac I, Šimić B, Barbir F. Experimental diagnostics and modeling of inductive phenomena at low frequencies in impedance spectra of proton exchange membrane fuel cells. J Power Sources 2017;365:240–8.
[22] Springer TE, Zawodzinski TA, Wilson MS, Gottesfeld S. Characterization of polymer electrolyte fuel cells using AC impedance spectroscopy. J Electrochem Soc 1996;143(2):587–99.
[23] Asghari S, Mokmeli A, Samavati M. Study of PEM fuel cell performance by electrochemical impedance spectroscopy. Pergamon: International Journal of Hydrogen Energy; 2010. p. 9283–90.
[24] Keller S, Özel T, Scherzer AC, Gerteisen Di, Groos U, Hebling C, Manoli Y. Characteristic time constants derived from the low-frequency arc of impedance spectra of fuel cell stacks. Journal of Electrochemical Energy Conversion and Storage 2018;15(2).
[25] Iranzo A, Muñoz M, Pino FJ, Rosa F. Non-dimensional analysis of PEM fuel cell phenomena by means of AC impedance measurements. J Power Sources 2011;196(9):4264–9.
[26] Malevich D, Halliop E, Peppley B, Pharoah J, Karan K. Effect of relative humidity on electrochemical active area and impedance response of PEM fuel cell. ECS Trans 2019;16(2):1763–74.
[27] Abe T, Shima H, Watanabe K, Ito Y. Study of PEFCs by AC impedance, current interrupt, and dew point measurements. J Electrochem Soc 2004;151(1):A101.
[28] Kim JH, Yeon Jo Y, Cho EA, Jang JH, Kim HJ, Lim T-H, Oh I-H, Ko JJ, Son IJ. Effects of cathode inlet relative humidity on PEMFC durability during startup–shutdown cycling. J Electrochem Soc 2010;157(5):B633.
[29] Holmström N, Wiezell K, Lindbergh G. Studying low-humidity effects in PEFCs using EIS. J Electrochem Soc 2012;159(8):F369–78.
[30] Schneider IA, Freunberger SA, Kramer D, Wokaun A, Scherer GG. Oscillations in gas channels: Part I. The forgotten player in impedance spectroscopy in PEFCs. J Electrochem Soc 2007;154(4):B383.
[31] Schneider IA, Kramer D, Wokaun A, Scherer GG. Oscillations in gas channels: II. Unraveling the characteristics of the low frequency loop in air-fed PEFC impedance spectra. J Electrochem Soc 2007;154(8):B770.
[32] Liu D, Lin R, Feng B, Yang Z. Investigation of the effect of cathode stoichiometry of proton exchange membrane fuel cell using localized electrochemical impedance spectroscopy based on print circuit board. Int J Hydrogen Energy 2019;44(14):7564–73.

Please cite this article as: Ghorbani B et al., Use of reduced-voltage EIS to establish a relation between oxygen concentration and EIS responses of large commercial PEM fuel cell modules, International Journal of Hydrogen Energy, https://doi.org/10.1016/j.ijhydene.2023.04.323

[33] Rezaei Niya SM, Phillips RK, Hoorfar M. Study of anode and cathode starvation effects on the impedance characteristics of proton exchange membrane fuel cells. J Electroanal Chem 2016;775:273–9.
[34] Petrone R, Vitagliano C, Péra M-C, Chamagne D, Sorrentino M. Characterization of an H_2/O_2 PEMFC short-stack performance aimed to health-state monitoring and diagnosis. Fuel Cell 2018;18(3):279–86.
[35] O'Rourke J, Ramani M, Arcak M. Using electrochemical impedance to determine airflow rates. Int J Hydrogen Energy 2008;33(17):4694–701.
[36] Chevalier S, Josset C, Bazylak A, Auvity B. Measurements of air velocities in polymer electrolyte membrane fuel cell channels using electrochemical impedance spectroscopy. J Electrochem Soc 2016;163(8):F816–23.
[37] Tsampas MN, Brosda S, Vayenas CG. Electrochemical impedance spectroscopy of fully hydrated nafion membranes at high and low hydrogen partial pressures. Pergamon: Electrochimica Acta; 2011. p. 10582–92.
[38] Niroumand AM, Mérida W, Eikerling M, Saif M. Pressure-voltage oscillations as a diagnostic tool for PEFC cathodes. Electrochem Commun 2010;12(1):122–4.
[39] Engebretsen E, Mason TJ, Shearing PR, Hinds G, Brett DJL. Electrochemical pressure impedance spectroscopy applied to the study of polymer electrolyte fuel cells. Electrochem Commun 2017;75:60–3.
[40] Li Y, Pei P, Wu Z, Ren P, Jia X, Chen D, Huang S. Approaches to avoid flooding in association with pressure drop in proton exchange membrane fuel cells. Appl Energy 2018;224:42–51.
[41] Dotelli G, Ferrero R, Stampino PG, Latorrata S, Toscani S. Diagnosis of PEM fuel cell drying and flooding based on power converter ripple. IEEE Trans Instrum Meas 2014;63(10):2341–8.
[42] Gebregergis A, Pillay P, Rengaswemy R. PEMFC fault diagnosis, modeling, and mitigation. In: Conference record - IAS annual meeting. IEEE Industry Applications Society; 2008.
[43] Hong P, Xu L, Jiang H, Li J, Ouyang M. A new approach to online AC impedance measurement at high frequency of PEM fuel cell stack. Int J Hydrogen Energy 2017;42(30):19156–69.
[44] Reshetenko T, Kulikovsky A. A model for extraction of spatially resolved data from impedance spectrum of a PEM fuel cell. J Electrochem Soc 2018;165(5):F291–6.
[45] Dotelli G, Ferrero R, Stampino PG, Latorrata S, Toscani S. PEM fuel cell drying and flooding diagnosis with signals injected by a power converter. IEEE Trans Instrum Meas 2015;64(8):2064–71.
[46] Kim J, Lee J, Cho BH. Equivalent circuit modeling of PEM fuel cell degradation combined with a LFRC. IEEE Trans Ind Electron 2013;60(11):5086–94.
[47] Cruz-Manzo S, Cano-Castillo U, Greenwood P. Impedance study on estimating electrochemical mechanisms in a polymer electrolyte fuel cell during gradual water accumulation. Fuel Cell 2019;19(1):71–83.
[48] Thomas A, Maranzana G, Didierjean S, Dillet J, Lottin O. Thermal effect on water transport in proton exchange membrane fuel cell. Fuel Cell 2012;12(2):212–24.
[49] Wiezell K, Holmström N, Lindbergh G. Studying low-humidity effects in PEFCs using EIS II. Modeling. J Electrochem Soc 2012;159(8):F379–92.
[50] Hink S, Roduner E. Application of a contact mode AFM for spatially resolved electrochemical impedance spectroscopy measurements of a nafion membrane electrode assembly. Phys Chem Chem Phys 2013;15(5):1408–16.
[51] Jiang R, Mittelsteadt CK, Gittleman CS. Through-plane proton transport resistance of membrane and ohmic resistance distribution in fuel cells. J Electrochem Soc 2009;156(12):B1440.
[52] Klingele M, Breitwieser M, Zengerle R, Thiele S. Direct deposition of proton exchange membranes enabling high performance hydrogen fuel cells. J Mater Chem 2015;3(21):11239–45.
[53] Atkinson RW, Rodgers JA, Hazard MW, Stroman RO, Gould BD. Influence of cathode gas diffusion media porosity on open-cathode fuel cells. J Electrochem Soc 2018;165(11):F1002–11.
[54] Liu X, Peng F, Lou G, Wen Z. Liquid water transport characteristics of porous diffusion media in polymer electrolyte membrane fuel cells: a review. J Power Sources 2015;299:85–96.
[55] Cindrella L, Kannan AM, Lin JF, Saminathan K, Ho Y, Lin CW, Wertz J. Gas diffusion layer for proton exchange membrane fuel cells-A review. J Power Sources 2009;194(1):146–60.
[56] Fadzillah DM, Rosli MI, Talib MZM, Kamarudin SK, Daud WRW. Review on microstructure modelling of a gas diffusion layer for proton exchange membrane fuel cells. Renewable and Sustainable Energy Reviews 2017;77:1001–9.
[57] Morgan JM, Datta R. Understanding the gas diffusion layer in proton exchange membrane fuel cells. I. How its structural characteristics affect diffusion and performance. J Power Sources 2014;251:269–78.
[58] Park J, Oh H, Ha T, Lee Y Il, Min K. A review of the gas diffusion layer in proton exchange membrane fuel cells: durability and degradation. Appl Energy 2015;155:866–80.
[59] Bultel Y, Wiezell K, Jaouen F, Ozil P, Lindbergh G. Investigation of mass transport in gas diffusion layer at the air cathode of a PEMFC. Electrochim Acta 2005;51(3):474–88.
[60] Li T, Wang K, Wang J, Liu Y, Han Y, Song J, Hu H, Lin G, Liu Y. Preparation of hierarchical-pore gas diffusion layer for fuel cell. J Mater Sci 2020;55(11):4558–69.
[61] Kong IM, Jung A, Kim MS. Investigations on the double gas diffusion backing layer for performance improvement of self-humidified proton exchange membrane fuel cells. Appl Energy 2016;176:149–56.
[62] Mukundan R, Lujan R, Davey JR, Spendelow JS, Hussey DS, Jacobson DL, Arif M, Borup R. Ice Formation in PEM fuel cells operated isothermally at sub-freezing temperatures. ECS Trans 2019;25(1):345–55.
[63] Liu H, George MG, Ge N, Muirhead D, Shrestha P, Lee J, Banerjee R, Zeis R, Messerschmidt M, Scholta J, Krolla P, Bazylak A. Microporous layer degradation in polymer electrolyte membrane fuel cells. J Electrochem Soc 2018;165(6):F3271–80.
[64] Lee Y, Kim B, Kim Y, Li X. Effects of a microporous layer on the performance degradation of proton exchange membrane fuel cells through repetitive freezing. J Power Sources 2011;196(4):1940–7.
[65] Jung G Bin, Tzeng WJ, Jao TC, Liu YH, Yeh CC. Investigation of porous carbon and carbon nanotube layer for proton exchange membrane fuel cells. Appl Energy 2013;101:457–64.
[66] Park S, Lee JW, Popov BN. Effect of carbon loading in microporous layer on PEM fuel cell performance. J Power Sources 2006;163:357–63. 1 SPEC. ISS.
[67] Antonacci P, Chevalier S, Lee J, Yip R, Ge N, Bazylak A. Feasibility of combining electrochemical impedance spectroscopy and synchrotron X-ray radiography for determining the influence of liquid water on polymer electrolyte membrane fuel cell performance. Int J Hydrogen Energy 2015;40(46):16494–502.
[68] Ozden A, Shahgaldi S, Li X, Hamdullahpur F. A graphene-based microporous layer for proton exchange membrane

Please cite this article as: Ghorbani B et al., Use of reduced-voltage EIS to establish a relation between oxygen concentration and EIS responses of large commercial PEM fuel cell modules, International Journal of Hydrogen Energy, https://doi.org/10.1016/j.ijhydene.2023.04.323

fuel cells: characterization and performance comparison. Renew Energy 2018;126:485–94.
[69] Kulikovsky AA. One-dimensional impedance of the cathode side of a PEM fuel cell: exact analytical solution. J Electrochem Soc 2015;162(3):F217–22.
[70] Kulikovsky A. Why impedance of the gas diffusion layer in a PEM fuel cell differs from the Warburg finite-length impedance? Electrochem Commun 2017;84:28–31.
[71] Cooper SJ, Bertei A, Finegan DP, Brandon NP. Simulated impedance of diffusion in porous media. Electrochim Acta 2017;251:681–9.
[72] Majlan EH, Rohendi D, Daud WRW, Husaini T, Haque MA. Electrode for proton exchange membrane fuel cells: a review. Renew Sustain Energy Rev 2018;89:117–34.
[73] Holdcroft S. Fuel cell catalyst layers: a polymer science perspective. Chem Mater 2014;26(1):381–93.
[74] Peron J, Shi Z, Holdcroft S. Hydrocarbon proton conducting polymers for fuel cell catalyst layers. Energy Environ Sci 2011;4(5):1575–91.
[75] Lefebvre MC, Martin RB, Pickup PG. Characterization of ionic conductivity profiles within proton exchange membrane fuel cell gas diffusion electrodes by impedance spectroscopy. Electrochem Solid State Lett 1999;2(6):259–61.
[76] Moghaddam RB, Easton EB. Impedance spectroscopy assessment of catalyst coated nafion assemblies for proton exchange membrane fuel cells. Electrochim Acta 2018;292:292–8.
[77] Liu Y, Ji C, Gu W, Baker DR, Jorne J, Gasteiger HA. Proton conduction in PEM fuel cell cathodes: effects of electrode thickness and ionomer equivalent weight. J Electrochem Soc 2010;157(8):B1154.
[78] Chen D, Kongkanand A, Jorne J. Proton conduction and oxygen diffusion in ultra-thin nafion films in PEM fuel cell: how thin? J Electrochem Soc 2019;166(2):F24–33.
[79] Paul DK, McCreery R, Karan K. Proton transport property in supported nafion nanothin films by electrochemical impedance spectroscopy. J Electrochem Soc 2014;161(14):F1395–402.
[80] Reshetenko T, Kulikovsky A. Impedance spectroscopy characterization of oxygen transport in low– and high–Pt loaded PEM fuel cells. J Electrochem Soc 2017;164(14):F1633–40.
[81] Lai Y-C, Huang K-L, Tsai C-H, Lee W-J, Chen Y-L. Sputtered Pt loadings of membrane electrode assemblies in proton exchange membrane fuel cells. Int J Energy Res 2012;36(8):918–27.
[82] Çögenli MS, Mukerjee S, Yurtcan AB. Membrane electrode assembly with ultra low platinum loading for cathode electrode of PEM fuel cell by using sputter deposition. Fuel Cell 2015;15(2):288–97.
[83] Pivac I, Bezmalinović D, Barbir F. Catalyst degradation diagnostics of proton exchange membrane fuel cells using electrochemical impedance spectroscopy. Int J Hydrogen Energy 2018;43(29):13512–20.
[84] Young AP, Stumper J, Gyenge E. Characterizing the structural degradation in a PEMFC cathode catalyst layer: carbon corrosion. J Electrochem Soc 2009;156(8):B913.
[85] Zhao J, Shahgaldi S, Li X, Liu Z, Simon). Experimental observations of microstructure changes in the catalyst layers of proton exchange membrane fuel cells under wet-dry cycles. J Electrochem Soc 2018;165(6):F3337–45.
[86] Pivac I, Bezmalinović D, Barbir F. Catalyst degradation diagnostics of proton exchange membrane fuel cells using electrochemical impedance spectroscopy. Int J Hydrogen Energy 2018;43(29):13512–20.
[87] Nara H, Tominaka S, Momma T, Osaka T. Impedance analysis counting reaction distribution on degradation of cathode catalyst layer in PEFCs. J Electrochem Soc 2011;158(9):B1184.
[88] Kulikovsky AA. Analytical solutions for polarization curve and impedance of the cathode catalyst layer with fast oxygen transport in a PEM fuel cell. J Electrochem Soc 2014;161(8):E3171–9.
[89] Kulikovsky AA. Exact low-current analytical solution for impedance of the cathode catalyst layer in a PEM fuel cell. Electrochim Acta 2014;147:773–7.
[90] Malevich D, Pharoah J, Peppley B, Karan K. On the determination of PEM fuel cell catalyst layer resistance from impedance measurement in H2/N2 cells. ECS Meeting Abstracts 2011;MA2011–02(16):1080.
[91] Aaron D, Yiacoumi S, Tsouris C. Effects of proton-exchange membrane fuel-cell operating conditions on charge transfer resistances measured by electrochemical impedance spectroscopy," *separation Science and technology*. Taylor & Francis Group; 2008. p. 2307–20.
[92] Shan J, Lin R, Chen X, Diao X. EIS and local resolved current density distribution analysis on effects of MPL on PEMFC performance at varied humidification. Int J Heat Mass Tran 2018;127:1076–83.
[93] Latorrata S, Pelosato R, Stampino PG, Cristiani C, Dotelli G. Use of electrochemical impedance spectroscopy for the evaluation of performance of PEM fuel cells based on carbon cloth gas diffusion electrodes. Journal of Spectroscopy 2018;2018:13 pages. Article ID 3254375.
[94] Homayouni H, DeVaal J, Golnaraghi F, Wang J. Voltage reduction technique for use with electrochemical impedance spectroscopy in high-voltage fuel cell and battery systems. IEEE Transactions on Transportation Electrification 2018;4(2):418–31.
[95] Ciucci F. Modeling electrochemical impedance spectroscopy. Current Opinion in Electrochemistry 2019;13:132–9.
[96] Zhai Y, Bethune K, Dorn S, Bender G, Rocheleau R. Electrochemical impedance spectroscopy analysis on SO 2 contamination in PEMFCs. ECS Trans 2019;28(23):313–23.
[97] Muralidharan VS. Warburg impedance - basics revisited. Anti-corrosion Methods & Mater 1997;44(1):26–9.
[98] Wagner N, Kaz T, Friedrich KA. Investigation of electrode composition of polymer fuel cells by electrochemical impedance spectroscopy. Electrochim Acta 2008;53(25):7475–82.
[99] Ren P, Pei P, Li Y, Wu Z, Chen D, Huang S, Jia X. Diagnosis of water failures in proton exchange membrane fuel cell with zero-phase ohmic resistance and fixed-low-frequency impedance. Appl Energy 2019;239:785–92.
[100] Hu B. Kramers-kronig in two lines. American Journal of Physics - AMER J PHYS 1989;57. 821–821.
[101] Poling BE, Prausnitz JM, O'connell JP, York N, San C, Lisbon F, Madrid L, City M, Delhi MN, Juan S. Properties of gases and liquids. McGraw-Hill Education; 2001.
[102] Shateri, M., Torabi, F., "Influence of liquid water accumulation on the impedance of a PEM fuel cell operating in dead end mode : physical modeling and experimental validation", Electrochim Acta, 443, pp. 141940.
[103] Li,H., Wei, W., Liu, F., Xu, X., Li, Z., Liu, Z., "Identification of internal polarization dynamics for solid oxide fuel cells investigated by electrochemical impedance spectroscopy and distribution of relaxation times", Energy, 267, pp. 126482.
[104] Pan, R., Hu, M., "Disclosure of the internal transport phenomena in the air-cooled proton exchange membrane fuel cell - part III: performance research based on qualitative comparisons between modeling and experimental results", Int J Hydrogen Energy, 47(9), pp. 6269-6281.

Please cite this article as: Ghorbani B et al., Use of reduced-voltage EIS to establish a relation between oxygen concentration and EIS responses of large commercial PEM fuel cell modules, International Journal of Hydrogen Energy, https://doi.org/10.1016/j.ijhydene.2023.04.323

[105] Tang, W., Chang, G., Yuan, H., Zhao, L., Liu, Z., Ming, P., Wei, X., Dai, H., "A novel multi-step investigation of in-plane heterogeneity for commercial-size fuel cells based on current distribution model and multi-point impedance method", Energy Conversion and Management, 272, pp. 116370.
[106] Yang, M., Jiang, Y., Liu, J., Xi, S., Du, A., "Lattice Boltzmann method modeling and experimental study on liquid water characteristics in the gas diffusion layer of proton exchange membrane fuel cells", Int J Hydrogen Energy, 47(18), pp. 10366-10380.
[107] Liu, D., Lin, R., Feng, B., Han, L., Zhang, Y., Ni, M., Wu, S., "Localised electrochemical impedance spectroscopy investigation of polymer electrolyte membrane fuel cells using Print circuit board based interference-free system", Appl Energy, 254, pp. 113712.
[108] Niroumand AM, Homayouni H, DeVaal J, Golnaraghi F, Kjeang E. In-situ diagnostic tools for hydrogen transfer leak characterization in PEM fuel cell stacks Part II: operational applications. J Power Sources 2016;322:147–54.

Please cite this article as: Ghorbani B et al., Use of reduced-voltage EIS to establish a relation between oxygen concentration and EIS responses of large commercial PEM fuel cell modules, International Journal of Hydrogen Energy, https://doi.org/10.1016/j.ijhydene.2023.04.323